# Time-dependent approach to inelastic scattering spectroscopies in and away from equilibrium: Beyond perturbation theory

Krissia Zawadzki, Luhang Yang, and Adrian E. Feiguin
*Department of Physics, Northeastern University, Boston, Massachusetts 02115, USA*

(Received 31 August 2020; accepted 8 December 2020; published 18 December 2020)

We propose a nonperturbative numerical approach to calculate the spectrum of a many-body Hamiltonian with time and momentum resolution by exactly recreating a scattering event using the time-dependent Schrödinger equation. Akin to an actual inelastic scattering experiment, we explicitly account for the incident and scattered particles (e.g., photons, neutrons, electrons, etc.) in the Hamiltonian and obtain the spectrum by measuring the energy and momentum lost by the particle after interacting with the sample. We illustrate the method by calculating the spin excitations of a Mott-insulating Hubbard chain after a sudden quench with the aid of the time-dependent density matrix renormalization group method. Our formalism can be applied to different forms of spectroscopies, such as neutron and Compton scattering and electron-energy-loss spectroscopy, for instance.

DOI: 10.1103/PhysRevB.102.235141

## I. INTRODUCTION

Inelastic scattering and, in general, energy-loss spectroscopies are exceptional tools that enables experimentalists to peek into the hidden mechanisms responsible for the magnetic and electronic excitations inside solids and molecules. For instance, the inelastic neutron scattering cross section is proportional to the magnetic dynamical structure factor [1–4], while Compton and electron-energy-loss (EELS) spectra are related to the charge density excitations [5–8]. In all these techniques, a sample is subjected to a beam of incident particles (neutrons, x-ray photons, and electrons, respectively, in the aforementioned cases), and the energy distribution of the scattered particles after they have interacted with the specimen is analyzed. In most cases, particles are able to penetrate several atomic layers before they are reflected, transferring part of their energy and momentum to the degrees of freedom in the material in the process. The corresponding information is gathered by measuring the energy and momentum "lost," which correspond, by conservation, to the energy and momentum transferred to the solid.

The foundations of time-dependent perturbation theory for quantum scattering are due to Schwinger and Lippman [9], who derived an expression for the scattering cross section as a linear response that accounts for the transition rate between the eigenstates as in Fermi's golden rule. If the system originally is in the ground state $|0\rangle$, this approach allows one to express the energy- and momentum-resolved spectral function as (we use units in which $\hbar = 1$)

$$S_O(\mathbf{k}, \omega) = 2\pi \sum_n |\langle n|O_{\mathbf{k}}|0\rangle|^2 \delta(\omega - E_n + E_0), \qquad (1)$$

where $\mathbf{k}$ represents the momentum quantum number, $|n\rangle$ are the eigenstates of the system's unperturbed Hamiltonian without the $V$ term with energy $E_n$, and $O_{\mathbf{k}}$ is the Fourier transform of the operator $O$ associated with the interaction potential between the incident particles and the degrees of freedom inside the sample (spin or electron density), which typically enters as a local contact term, as we describe in the next section.

The relative simplicity of the previous expression has allowed theorists and experimentalists to model and compare predictions with theory very accurately. In the particular context of strongly correlated quantum matter, these calculations are carried out by means of state-of-the-art computational techniques. These include exact diagonalization [10], which is limited to small system sizes; quantum Monte Carlo, which is conditioned by the sign problem and requires uncontrolled analytic continuations and the use of the max entropy approximation [11–18]; the dynamical density matrix renormalization group (DMRG) [19–21], which is computationally demanding and applies mostly to quasi-one-dimensional systems; the time-dependent DMRG [22–27]; and recent variations using Chebyshev expansions [28–30], also limited by the entanglement growth. In addition, matrix product states have been used to build variational forms for excited states [31,32]. Similar ideas were explored with variational Monte Carlo, which can easily be extended to higher dimensions and is free from the sign problem [33–36].

Despite their success, these methods hit a hard wall when it comes to studying dynamics of a system far from equilibrium, as a result of a pump or a quench, for instance. In that case, it is appropriate to assume that the system is initially in a generic state $|\phi\rangle = \sum_n a_n |n\rangle$. The expression for the spectral function is now given as [37]

$$S_O(k, \omega, t) = 4\pi^2 \sum_m \left| \sum_n a_n \langle m|O|n\rangle \delta^t(\omega - \omega_{mn}) \right|^2, \qquad (2)$$

 

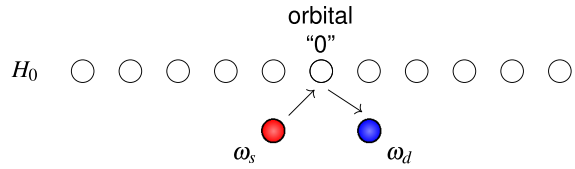


FIG. 1. Scattering process of a single particle in one dimension.

where we have introduced the time dependence in the definition

$$\delta^t(\omega) = \frac{1}{\pi}\frac{\sin(\omega t/2)}{\omega} \underset{t\to\infty}{\to} \delta(\omega). \tag{3}$$

Unlike the equilibrium case, this expression cannot be simplified, and at the same time, most methods listed above no longer apply [37–39], forcing us to rely on the limited power of exact diagonalization.

The aim of this work is to compute the spectrum of energy-loss spectroscopies without resorting to perturbation theory or to the calculation of the full eigenspectrum of the system. Working directly in the time domain, we propose to simulate the entire scattering event by solving the time-dependent Schrödinger equation for an equivalent system comprising the sample, a source, and a detector. The interaction terms between incident and reflected particles are included explicitly, and a response function for the detector can be calculated exactly in real time. In this scenario, the spectrum can be conveniently obtained with low computational effort using the time-dependent DMRG (TDMRG). Besides the obvious numerical advantages, our method is able to reveal features in the scattering spectrum that remain hidden in the conventional perturbative expression obtained from the linear response.

Our paper is organized as follows: In Sec. II, we present the mathematical formulation and the numerical scheme used to simulate the scattering event using the time-dependent DMRG method. In Sec. III, we show numerical results for the Heisenberg chain and the Hubbard chain in and away from equilibrium. We finally close with a discussion.

## II. METHOD

In "energy-loss" spectroscopies an incident particle (photon, neutron, electron) with initial energy $\omega_s$ interacts with a system described by a Hamiltonian $H_0$ and is inelastically reflected with final energy $\omega_d$, typically off resonance. In an actual experiment, the energies $\omega_s = k_s^2/2m$ and $\omega_d = k_2^2/2m$ correspond to the kinetic energy of free particles (neutrons, electrons) in the beam (obviously, these expressions do not apply to photons). Conservation laws imply that the energy lost by the particle has been transferred to the system $\Delta E = \omega_d - \omega_s$ (see Fig. 1). As mentioned in the Introduction, the measurement of the cross section of the outgoing particle is directly related to the excitation spectrum of the sample.

To model this process we consider the Hamiltonian

$$H = H_0 + H_d + V, \tag{4}$$

where $H_0$ is the Hamiltonian for the system of interest characterized by the energy scale $J$ and

$$H_d = \omega_s n_s + \omega_d n_d \tag{5}$$

represents the energy of a particle coming in with energy $\omega_s$ and going out with energy $\omega_d$. From now on we will refer to the "orbitals" representing these two states as "source" and "detector"/"probe," respectively. The term $V$ is a "contact" interaction between the particles and the sample that remains to be determined, depending on the nature of the spectroscopy of interest.

For simplicity, let us first focus on the energy spectrum without momentum resolution. In this case, the contact term acts only on a site that we label 0. We assume that there is no absorption and the incident particle can only be reflected.

We want to represent a single-particle scattering event, in which, initially, orbital $s$ is occupied, while $d$ is empty. The term $V$ is responsible for making the particle undergo a transition from a state with energy $\omega_s$ to a state with final energy $\omega_d$ due to either the Coulomb interaction or some other effect. In the case in which the force is of electrostatic origin, the potential is described as

$$\begin{aligned} V &= J' n_0 (n_s + n_d)(c_s^\dagger c_d + \text{H.c.}) \\ &= J' n_0 (c_s^\dagger c_d + \text{H.c.}), \end{aligned} \tag{6}$$

where $n_0$, $n_s$, and $n_d$ are the occupation numbers of the system's orbital 0, source, and detector, respectively. Since the particle can be in only the source or the detector, $n_s + n_d = 1$ is a constraint and must be satisfied at all times. Note that the creation and annihilation operators in this expression can be either bosonic or fermionic since there is only one such particle and its nature does not play a role. The constant $J'$ is a matrix element that will depend on the particular details of the electronic wave function. The calculation of $J$ is referred to as the "matrix elements" problem, and in the following we assume $J'$ is a small constant.

For the case of neutrons interacting via (longitudinal) spin interactions, the perturbation can be expressed as

$$V = J' S_0^z (c_s^\dagger c_d + \text{H.c.}), \tag{7}$$

where the constraint is now $S_s^z + S_d^z = 1/2$. Note that the scenario in which the probe particles are photons requires more care because it involves the creation and annihilation of particles [40].

We now have all the ingredients to measure the energy loss of the particle after the scattering event.

At time $t = 0$, we consider the total wave function of the system to be

$$|\Psi(t=0)\rangle = |\phi\rangle \otimes |n_s = 1\rangle \otimes |n_d = 0\rangle\,, \tag{8}$$

where $|\phi\rangle$ is the state of the sample (in or away from equilibrium) and $|n_s\rangle$ and $|n_d\rangle$ describe the states for the source and detector, respectively.

Then, the coupling $J'$ is turned on, and the full Hamiltonian including the scattering terms is evolved in time. The occupation of the detector $\langle n_d(t)\rangle$ will be proportional to the spectral density at energy $\omega_d$, as $S_O(\omega_d) \propto \lim_{t\to\infty} n_d(t)/t$. One can easily show (see the Appendix) that, in the limit $J' \ll J$, one recovers the same result as that obtained from perturbation theory. As we shall discuss later, in the implementation, three important details require special attention: (i) The full spectrum is recovered only after scanning $\omega_d$ over an energy range. (ii) In our scheme with just one source and probe orbitals, at

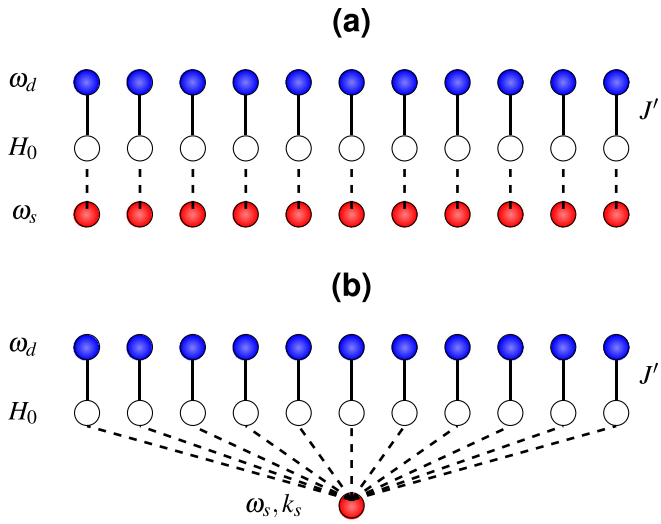


FIG. 2. Possible geometries used in simulating a scattering event of a single particle with a 1D sample: (a) chain geometry in real space and (b) star in momentum space. The open circles represent the sample orbitals, while red (blue) solid circles indicate the source (detector) orbitals for the incident and scattered particles, respectively. Orbitals connected by lines interact via the perturbation $V$.

sufficiently long times, the particle oscillates back and forth between the two. Hence, the $t \to \infty$ limit is not well defined. (iii) Finally, since the treatment of the interaction does not rely on perturbation theory, the measure $\langle n_d(t)\rangle$ will contain all contributions to all orders.

### A. Momentum resolution

To adapt the previous ideas to translationally invariant systems, we now model the source and detector to account for the momentum of the incoming and outgoing particle. For illustration and simplicity, we limit our discussion to the one-dimensional case, but the same considerations can be generalized to any geometry. Below, we present two alternative, but equivalent, forms that will yield similar results but will differ in their implementation.

#### *1. Chain geometry*

We first describe what we refer to as the "chain geometry" [37]: Both the source and detector are represented as two parallel chains of orbitals with the same number of "sites" as the system under study, represented by Hamiltonian $H_0$, as shown in in Fig. 2(a).

The Hamiltonian $H_d$ is now given by

$$H_d = \omega_s \sum_\ell n_{s\ell} + \omega_d \sum_\ell n_{d\ell}, \tag{9}$$

and the interaction between the system and the source is written as

$$V = J' \sum_\ell O_\ell (c^\dagger_{s\ell} c_{d\ell} + \text{H.c.}), \tag{10}$$

where $O_\ell$ is some generic diagonal local operator acting on site $\ell$ (we consider $O_\ell = O^\dagger_\ell$, but the formalism can be generalized to other cases).

Since the source, probe, and system are extended in space and the interaction term is invariant under translations, momentum conservation is ensured. In the present setup, the initial state of the full system is given by

$$|\Psi(t=0)\rangle = |\phi\rangle \otimes |n_s = 1, k_s = k_0\rangle \otimes |n_d = 0\rangle\,, \tag{11}$$

where $k_0$ is the momentum of the incident particle at the source.

By measuring the momentum distribution at the detector $n_{dk}(t)$,

$$n_{dk}(t) = \frac{1}{L} \sum_{\ell,\ell'} e^{ik(\ell-\ell')} \langle c^\dagger_{d\ell} c_{d\ell'}(t)\rangle, \tag{12}$$

we obtain the full spectrum of the system with both time and momentum resolution.

#### *2. Star geometry*

The number of degrees of freedom can be reduced considerably by accounting explicitly for the fact that the incident particle can assume only one allowed value of momentum $k_0$. In this case, instead of representing the source by a chain, we do it as a single orbital with energy $\omega_s$ and momentum $k_0$. In our approach, we fix the source to have the same momentum as the incident particle $k_0 = k_s$ in the beginning of the calculation. Therefore, the Hamiltonian $H_d$ becomes

$$H_d = \omega_s n_{sk_0} + \omega_d \sum_\ell n_{d\ell}, \tag{13}$$

and the interaction

$$V = \frac{J'}{\sqrt{L}} \sum_\ell O_\ell \left(e^{ik_0\ell} c^\dagger_{d,\ell} c_{s,k_0} + \text{H.c.}\right), \tag{14}$$

with $O_k = 1/L \sum_\ell e^{ik\ell} O_\ell$. The corresponding geometry is illustrated in Fig. 2(b). Notice that while the complexity of the problem has been greatly reduced, the Hamiltonian now contains long-range terms.

Finally, we point out that, besides the two described approaches, there is yet a third possibility: a "double-star" geometry in which the probe is "tuned" to detect only a scattered particle with fixed momentum $k_d$. In this case, we find that the interaction would be written as

$$V = \frac{J'}{L} \sum_\ell O_\ell \left(e^{i(k_0-k_d)\ell} c^\dagger_{d,k_d} c_{s,k_0} + \text{H.c.}\right). \tag{15}$$

When using this scheme, one needs to carry out one calculation for each value of $k_d$, increasing the computational overhead by a factor of $L$.

### B. DMRG implementation

In order to recast these ideas into a practical numerical solver, we will describe implementation in the context of the time-dependent DMRG method. For this purpose, we consider a chain with $L$ sites coupled to two auxiliary chains $s$ and $d$ accounting for the source and detector or probe of neutrons, electrons, or photons. The main advantage of this setup, compared to the star geometries is that the Hamiltonian remains local and allows for a straightforward Suzuki-Trotter decomposition of the evolution operator (for details about

TDMRG we direct the reader to [23,25,27]). As examples, we shall present two cases for prototypical Hamiltonians $H_0$: The Hubbard chain is defined as

$$H_{\text{Hubbard}} = -J \sum_{i=1,\sigma}^{L-1} (c_{i\sigma}^{\dagger} c_{i+1\sigma} + \text{H.c.}) + U \sum_{i=1}^{L} \left(n_{i\uparrow} - \frac{1}{2}\right)\left(n_{i\downarrow} - \frac{1}{2}\right), \quad (16)$$

where $U$ and $J$ parametrize the on-site Coulomb interaction and the hopping, respectively (the symbol $t$ is reserved for the time variable). In the large-$U/J$ limit, the charge fluctuations are suppressed, and only the spin degree of freedom remains. In this regime, the low-energy physics is well described by the one-dimensional Heisenberg model:

$$H_{\text{Heis}} = J_H \sum_i \vec{S}_i \cdot \vec{S}_{i+1}, \quad (17)$$

where the operators $\vec{S}$ represent $S = 1/2$ spins and $J_H \sim 4J^2/U$.

Without loss of generality, we use a spinless fermion to represent the incident and scattered particles.

For ground-state calculations, we use the conventional DMRG method to initialize the system. To ensure that the source particle is in a state with a well-defined momentum and that the detector is empty, we include a projector $H_{k_0} = |k_0\rangle\langle k_0|$ and a large positive potential term in the detector. Alternatively, the chain can be in a state far from equilibrium, resulting from a quench or a pump, for instance. In either case, before the measurement starts, the scattering term is always "turned off" with $J' = 0$. At $t = 0$ the source and probe are connected, and one can start measuring the momentum distribution on the detector chain. This procedure is carried out by keeping enough DMRG states to ensure a truncation error of the order of $10^{-6}$, corresponding to a block dimension up to $m = 400$ in the worst cases. We typically run the simulations to times of the order of $t_{\text{probe}} = 50$ (in units of $J^{-1}$) for each energy $\omega_d$. This represents hundreds of simulations, but they are all carried out in parallel independently.

In our work we assume that $J'$ is a small constant, thus allowing us to recover the usual expressions in perturbation theory, i.e., small enough such that we remain in the perturbative regime. Otherwise, the incident particle can become more than a probe, either by entangling with the system or by inducing a physics in the sample different from the one we intend to observe. In addition, a compromise must be reached in order to obtain decent visibility in relatively accessible simulations times. Unless otherwise stated, we use $J' = 0.2$ in the rest of the paper.

## III. RESULTS

### A. Heisenberg chain

As a control case study, we first calculate the spectrum of a spin chain (17) with $J_H = 1$ as our unit of energy. The one-dimensional Heisenberg model does not realize long-range order, and the antiferromagnetic correlations decay algebraically. In additions, the model displays spinon excitations (domain walls) that carry spin 1/2. The spectrum

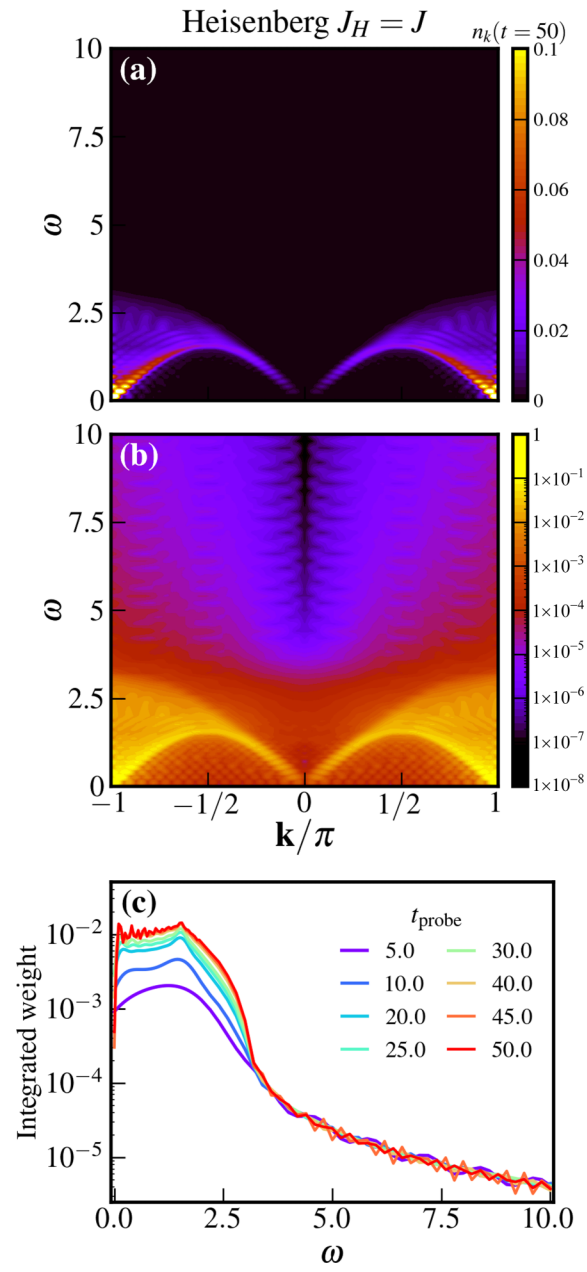


FIG. 3. Momentum-resolved neutron scattering spectrum of Heisenberg chains of size $L = 32$ at the final time $t_{\text{probe}}J = 50$. Color scales are (a) linear and (b) logarithmic. (c) Integrated weight.

is gapless and bounded from below by the des Cloizeaux–Pearson dispersion $\pi J/2|\sin k|$ [41], and the upper boundary of the continuum is $\pi J|\sin(k/2)|$ [42]. This physics is realized in a number of quasi-one-dimensional magnets, and the spinon excitations have been experimentally confirmed [43–57]. Since spinons are not conventional Landau quasiparticles, the spectrum exhibits singularities at the edges instead of a coherent band or dispersion. We show results at time $t = 50$ in Fig. 3; Figs. 3(a) and 3(b) display the momentum-resolved spin dynamical spectral function obtained with our approach in linear and log scales, respectively, while Fig. 3(c) shows the integrated weight. The oscillations in Fig. 3(c) are due to the high resolution of the measurement, which reveals

finite-size effects since we are considering a finite chain of length $L = 32$ (in finite systems the spectrum is a collection of $\delta$ peaks). It is possible that the very faint spectral weight at high energies seen in the log scale [Figs. 3(b) and 3(c)] originates from multispinon excitations. However, since these features are at the limit of our numerical resolution and are orders of magnitude smaller than the two-spinon continuum, we cannot support any claims in that direction.

Figure 3(c) illustrates the convergence of the spectrum as time evolves. At short measuring times, the features are broader and less resolved, a manifestations of the energy-time uncertainty principle. At very long times, the scattering particle indeed will undergo "Rabi-like" oscillations between the source and drain. Therefore, the measurement has to be carried out during the first "tunneling" event, which describes the actual impact with the sample. Any subsequent occurrences are artifacts of the present setup. However, this behavior is not observed in the simulation times considered in this work. The optimal measuring time is determined *ad hoc* as the one corresponding to maximum visibility, which translates into maximum amplitude of the edges of the spectrum and smaller broadening of the main features. As one can observe, the resolution increases with time, as expected. As a matter of fact, in most of the cases presented in this paper, the spectrum just keeps getting sharper and sharper as time evolves. In practice, one can stop the simulation when the resolution is satisfactory.

### B. Hubbard chain

The Hubbard chain at half filling is a Mott insulator with a charge gap that increases with $U/J$. However, spin excitations remain gapless and are also spinons, with a dispersion that resembles the one for the spin chain, but with a renormalized coupling $J_H \sim 4J^2/U$ [58]. The results of our calculations are shown in Figs. 4 and 5 for $U/J = 4$ and 8, respectively. In both cases, the hopping $J = 1$ is our unit of energy. We observe a well-defined spinon spectrum with a bandwidth determined by the renormalized value of $J_H$. However, in the $U/J = 4$ case, an unexpected "bubble" of spectral weight is discerned above the continuum at energies near $\omega \sim 2.5$. These features are enhanced and clearly visible in the log-scale plot [Fig. 4(b)]. Furthermore, the extra spectral weight can be appreciated in the integrated spectral density [Fig. 4(c)]. By paying further attention, we discover similar features in the $U/J = 8$ results that, albeit being fainter than in the previous case, become obvious also in log scale and occur at higher energies. This high-energy bubble does not appear in calculations using linear response, Eq. (2), begging us to try to understand its origin.

In order to identify the high-energy features, we resort to exact diagonalization calculations for small systems. In Fig. 6 we show the eigenvalues for a chain with $L = 10$ sites with total spin $S = 0$ and $U/J = 4$ [Fig. 6(a)] and $U/J = 8$ [Fig. 6(b)]. We observe that, besides the low-energy manifold describing the spin physics traditionally associated with the Heisenberg limit, we also find a high-energy manifold separated by a gap (the Mott gap). These states correspond to spin excitations in the upper Hubbard band. Why do they appear in our spectrum? To answer this question we recall

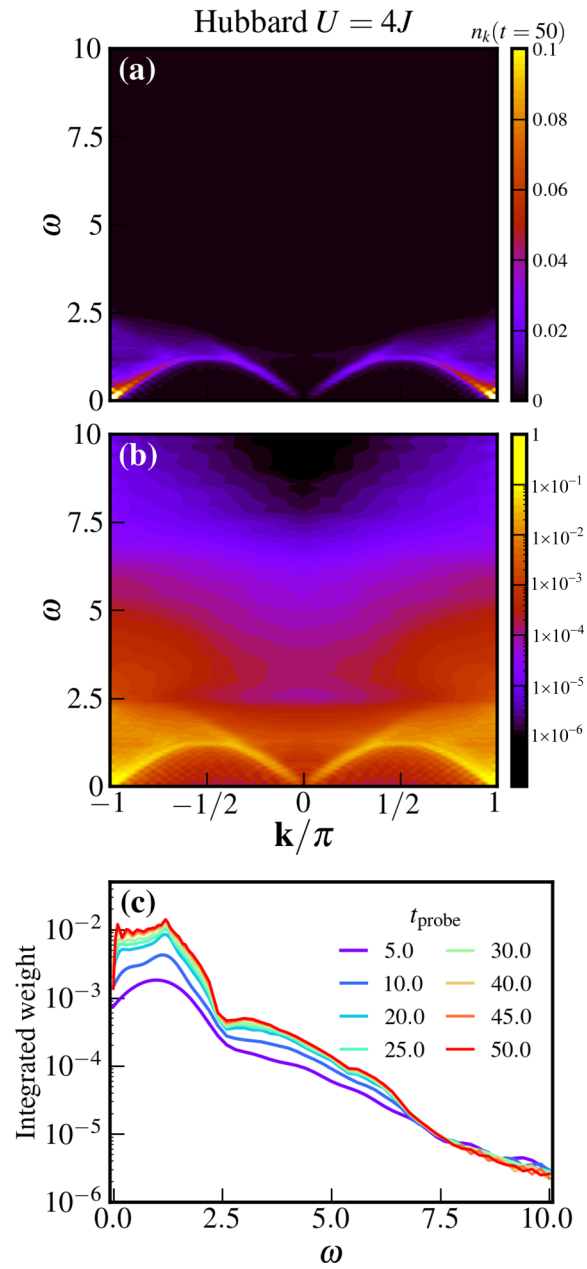


FIG. 4. Neutron scattering spectrum of half-filled Hubbard chains of size $L = 32$ with Coulomb coupling $U/J = 4.0$. Momentum-resolved spectrum at final time $tJ = 50$ is plotted on (a) linear and (b) logarithmic color scales. (c) Integrated weight.

that our formulation does not rely on perturbation theory, and therefore, it contains all contributions to $n_{dk}$ to all orders. Therefore, the appearance of the new features can be associated with high-order contributions that, we should emphasize, are real in the sense that an idealized experimental setup with high resolution and no noise should be able to resolve them, particularly if the matrix elements (our $J'$) are large. However, despite this fact, this spectral weight is not associated with the spectral function (a quantity that arises from linear response), but to higher-order transitions.

It turns out that similar contributions can be observed in the low-energy spectrum, as shown in Fig. 7. We here compare the

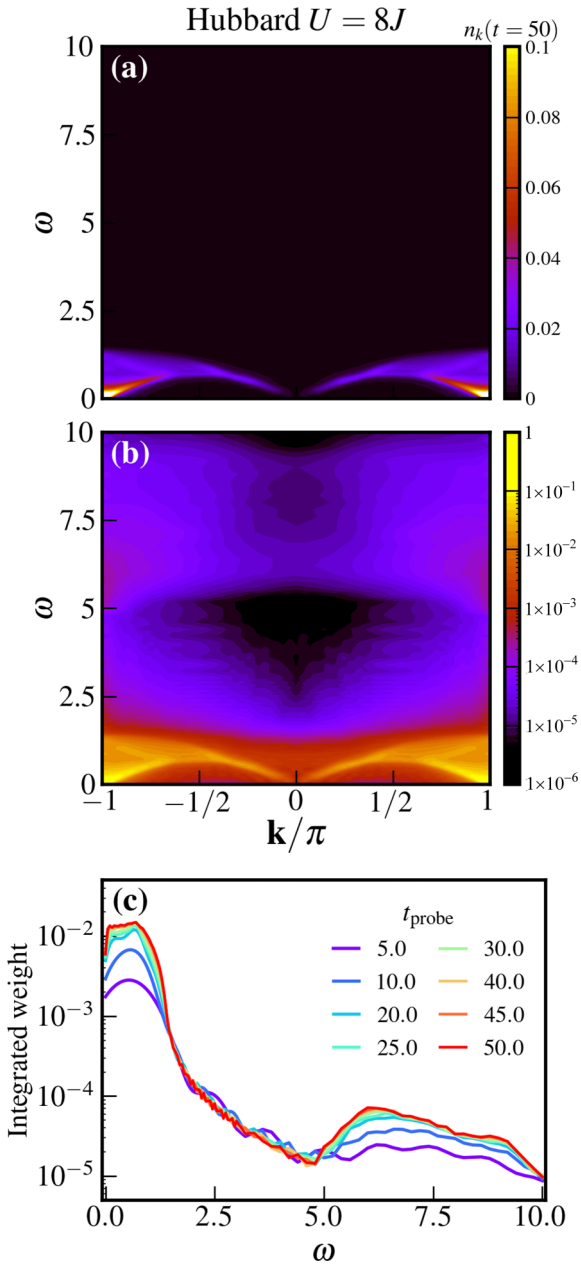


FIG. 5. Same as Fig. 4, but for $U/J = 8$.

results obtained by means of our scattering approach and the spectral function $S(k, \omega)$ obtained from equilibrium Green's functions using TDMRG [23,25,27]. While the spectral function $S(k, \omega)$ displays a sharp lower edge, the higher-order contributions are evident in the inelastic scattering spectrum with the appearance of a new "branch" in the middle of the continuum and a drop in the spectral weight at the low-energy edge of the spectrum between $k = 0$ and $k \approx 2/3\pi$.

### C. Hubbard chain after a quench

We now proceed to study the case of a Hubbard chain far from equilibrium after a sudden quench in $H_{\text{Hubbard}}$ from $U_0/J = 0$ to $U/J = 8$. At $t = 0$, the initial state is the ground state of the noninteracting Hamiltonian. We then suddenly change the value of the interactions to $U/J = 8$, and we

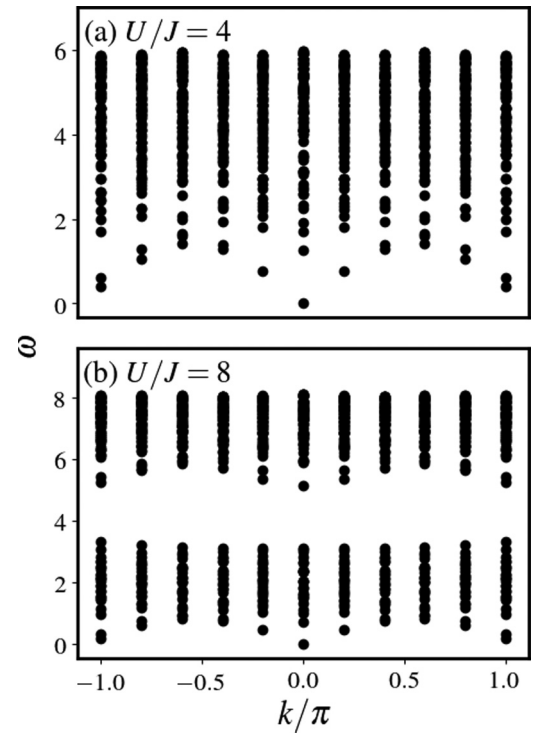


FIG. 6. Exact spectrum for a half-filled Hubbard chain with $L = 10$ sites in the $Sz = 0$ subspace for (a) $U/J = 4$ and (b) $U/J = 8$.

measure the spectrum of the system in the resulting nonthermal state of the new interacting Hamiltonian. Much attention has been paid to the problem of the "melting" of the Mott insulator [37,59–71], mostly in the context of the photoemission response. By pumping energy into the system, one can change the population of doublons and induce excitations into the upper Hubbard band. The effects of the quench are similar to photodoping: The chain is no longer insulating but will have a finite density of holes and double-occupied sites that will differ from that in equilibrium (essentially, the equivalent to particle-hole excitations in a Mott insulator). As a result, the chain will be gapless for both the spin and charge sectors. This

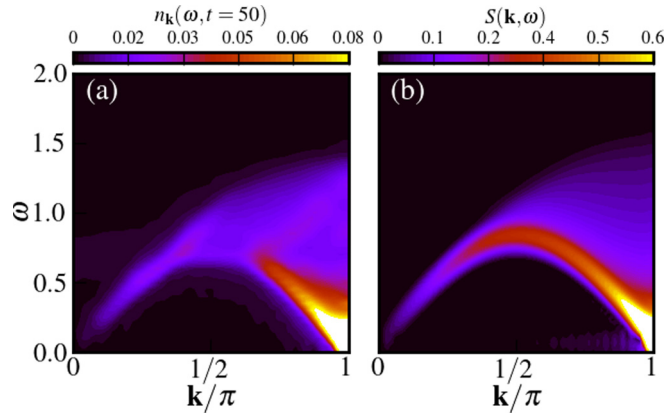


FIG. 7. Comparison between (a) the nonperturbative time-dependent scattering approach introduced in this work and (b) equilibrium Green's function results for a Hubbard chain with $U/J = 8$ using TDMRG (in arbitrary units).

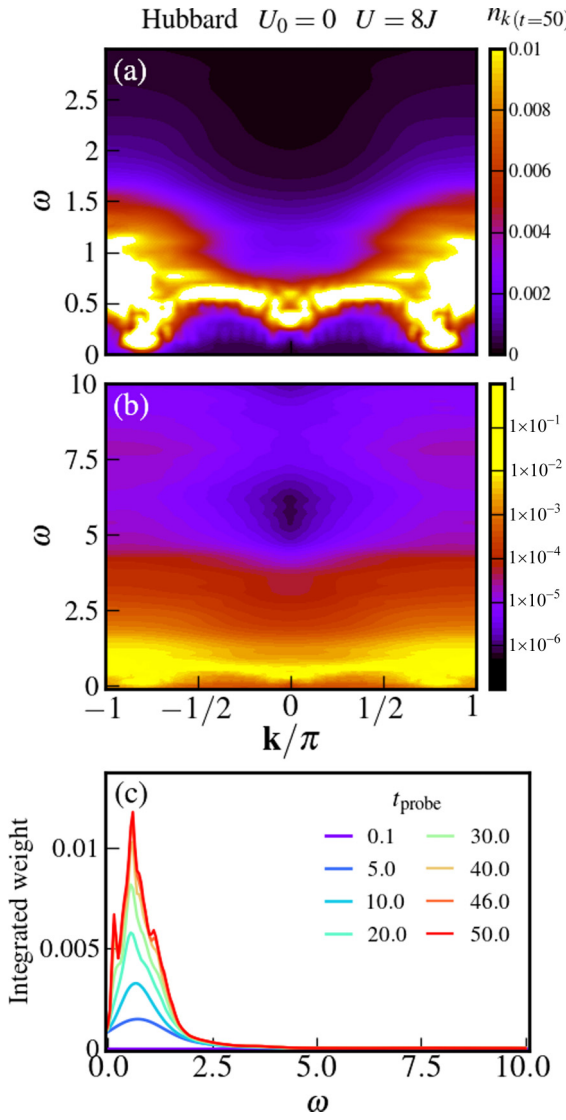


FIG. 8. Neutron scattering spectrum of a Hubbard chain quenched from $U_0/J = 0$ to $U/J = 8$. Momentum-resolved spectrum on (a) linear and (b) logarithmic color scales. (c) Integrated weight as a function of probing times.

will be reflected in the spectrum probed by neutron scattering, which now will display a superposition of coexisting spin excitations in the upper and Hubbard bands, as shown in our results (Fig. 8). Interestingly, the high-energy bubble has also melted, together with the Mott gap. Consequently, the magnetic order (or "quasiorder" in one dimension) has also been modified: The signatures of "$2k_F$" singularities are no longer well defined, and we see indications of gapless dispersive branches shifted away from $k = \pi$, as expected from a doped Mott insulator [71,72]. In a nonequilibrium, nonthermal state such as the one realized in a quench, the concepts of bands and dispersion are not well defined in the conventional sense. The measured spectrum contains contributions from all allowed transitions $\omega_{mn} = E_m - E_n$ and will typically appear as an incoherent continuum.

## IV. CONCLUSIONS

We have presented a numerical approach to calculate inelastic scattering spectra by directly simulating a scattering event using the time-dependent Schrödinger equation. Unlike conventional approaches that rely on evaluating Green's functions in the frequency or time domain, we directly obtained the spectral density through the probability of detecting an event after an incident particle is deflected from the sample. The method not only reproduces the energy- and momentum-resolved results from equilibrium Green's functions but includes contributions to all orders, revealing hidden features that can potentially be observed experimentally. These higher-order features correspond to transitions between excited states. Their visibility depends on the magnitude of the coupling between the incident particles and the sample (the so-called matrix elements) and the intensity of the beam. For weak interactions (smaller $J'$) they will be rapidly suppressed since the next correction enters with a $J'^3$ prefactor. In terms of practicality in the context of numerical calculations, a smaller $J'$ implies a broadening in the spectral features for the same $t_{\text{probe}}$, meaning that we need to increase the simulation time to achieve the same resolution. The noteworthy aspect of this method is that, by circumventing the direct explicit evaluation of matrix elements between excited states, the approach can be readily and seamlessly applied to nonequilibrium problems that would otherwise be out of reach for conventional numerical alternatives.

## ACKNOWLEDGMENTS

We thank F. Essler and I. Zaliznyak for illuminating discussions and carefully reading the manuscript. We acknowledge generous computational resources provided by Northeastern University's Discovery Cluster at the Massachusetts Green High Performance Computing Center (MGHPCC). K.Z. is supported by a Faculty of the Future fellowship of the Schlumberger Foundation. A.E.F. and L.Y. are supported by the US Department of Energy, Office of Basic Energy Sciences, under Grant No. DE-SC0014407. K.Z. is partially supported by the same grant.

## APPENDIX: PERTURBATIVE ANALYSIS OF THE RESPONSE FUNCTIONS

### 1. Local probe

For simplicity, we first describe the local case in which a particle hits the sample at position 0 and interacts locally with the electrons via a local Coulomb term (effectively describing an EELS event). The first contribution to the number of particles with energy $\omega_d$ in the detector can be calculated as

$$\langle n_d(t)\rangle = \int_0^t dt_1 \int_0^t dt_2 \langle e^{i(H_0+H_d)t_1} V e^{-i(H_0+H_d)t_1} n_d e^{i(H_0+H_d)t_2} V e^{-i(H_0+H_d)t_2}\rangle. \tag{A1}$$

The action of $V$ on the initial state is very simple. Assuming that the system is initially in equilibrium in the ground state,

$$V\,|\Psi(t=0)\rangle = J' n_0\,|gs\rangle\,|n_s=0, n_d=1\rangle\,, \tag{A2}$$

and Eq. (A1) becomes

$$\begin{aligned}
\langle n_d(t)\rangle &= J'^2\int_0^t dt_1\int_0^t dt_2 e^{i(E_0+\omega_s)(t_1-t_2)}\,\langle gs|\,\langle 0,1|\,n_0 e^{-i(H_0+H_d)t_1} n_d e^{i(H_0+H_d)t_2} n_0\,|gs\rangle\,|0,1\rangle \\
&= J'^2\int_0^t dt_1\int_0^t dt_2 e^{i(E_0+\omega_s)(t_1-t_2)} e^{-i\omega_d(t_1-t_2)}\,\langle gs|\,n_0 e^{-iH_0(t_1-t_2)} n_0\,|gs\rangle \\
&= J'^2\int_0^t dt_1\int_0^t dt_2\sum_{|f\rangle} e^{i(E_0+\omega_s-\omega_d)(t_1-t_2)} e^{-iE_f(t_1-t_2)}|\langle gs|\,n_0\,|f\rangle|^2 \\
&= J'^2\int_0^t dt_1\int_0^t dt_2\sum_{|f\rangle} e^{i[(E_0-E_f)+(\omega_s-\omega_d)](t_1-t_2)}|\langle gs|\,n_0\,|f\rangle|^2 \\
&= 4J'^2\sum_{|f\rangle}\frac{\sin^2\{[\omega-(E_0-E_f)]t/2\}}{[\omega-(E_0-E_f)]^2}|\langle gs|\,n_0\,|f\rangle|^2,
\end{aligned} \tag{A3}$$

where $\omega=\omega_s-\omega_d$. In the limit of $t\to\infty$ it can be written as

$$\frac{\langle n(t)\rangle}{t}\to 2\pi\sum_{|f\rangle}|\langle gs|\,n_0\,|f\rangle|^2\delta[\omega-(E_0-E_f)]. \tag{A4}$$

Note that in the case of neutron scattering, we can replace the term $n_0(n_s+n_d)$ in $V$ by $S_0^z(S_1^z+S_2^z)=1/2S_0^2$, so that the observable in the brackets in the last line of Eq. (A3) is given by $S_0^z$.

### 2. Extended probe: Momentum resolution

We generalize the previous case to an extended probe with momentum resolution and an arbitrary contact term in the potential with an operator $O$. The signal at the detector is now the momentum distribution function, which can be obtained as

$$\langle n_{2k}(t)\rangle = \int_0^t dt_1\int_0^t dt_2\langle e^{i(H_0+H_d)t_1} V e^{-i(H_0+H_d)t_1} n_{2k} e^{i(H_0+H_d)t_2} V e^{-i(H_0+H_d)t_2}\rangle. \tag{A5}$$

We assume that at $t=0$ the system is in equilibrium in the ground state; hence,

$$\langle n_{2k}(t)\rangle = \int_0^t dt_1\int_0^t dt_2 e^{i(E_0+\omega_s)(t_1-t_2)}\,\langle gs|\,\langle k_0,0|\,V e^{-i(H_0+H_d)t_1} n_{2k} e^{i(H_0+H_d)t_2} V\,|gs\rangle\,|k_0,0\rangle\,. \tag{A6}$$

Applying $V$ to $\Psi(t=0)$ yields

$$\begin{aligned}
V\,|gs\rangle\,|k_0,0\rangle &= \frac{J'}{L}\sum_\ell O_\ell\,|gs\rangle\sum_{q,p} e^{i(p-q)\ell} c_{2p}^\dagger c_{1q}\,|k_0,0\rangle \\
&= \frac{J'}{L}\sum_\ell\sum_p e^{i(p-k_0)\ell} O_\ell\,|gs\rangle\,|0,p\rangle\,.
\end{aligned} \tag{A7}$$

In addition, $n_{2k}$ projects the state onto one with well-defined momentum:

$$n_{2k} V\,|gs\rangle\,|k_0,0\rangle = \frac{J'}{L}\sum_\ell e^{i(k-k_0)\ell} O_\ell\,|gs\rangle\,|0,k\rangle = J' O_{k-k_0}\,|gs\rangle\,|0,k\rangle\,. \tag{A8}$$

Taking that into consideration, expression (A6) becomes

$$\langle n_{2m}(t)\rangle = J'^2\sum_f\int_0^t dt_1\int_0^t dt_2 e^{i(E_0-E_f+\omega_s-\omega_d)(t_1-t_2)}|\langle f|\,O_{k-k_0}\,|gs\rangle|^2. \tag{A9}$$

In this expression we recognize the momentum-resolved spectral function for operator $O$, shifted by $k_0$

$$\langle n_{2m}(t)\rangle = 4J'^2\sum_{|f\rangle}\frac{\sin^2\{[\omega-(E_0-E_f)]t/2\}}{[\omega-(E_0-E_f)]^2}|\langle gs|\,O_{k-k_0}\,|f\rangle|^2. \tag{A10}$$

[1] H. Schober, J. Neutron Res. **17**, 109 (2014).
[2] A. Furrer, J. Mesot, and T. Strässle, *Neutron Scattering in Condensed Matter Physics* (World Scientific, Singapore, 2010).
[3] S. W. Lovesey, *Theory of Neutron Scattering from Condensed Matter Physics* (Oxford University Press, Oxford, 2003), Vol. 2.
[4] I. A. Zaliznyak and J. M. Tranquada, in *Strongly Correlated Systems: Experimental Techniques*, edited by A. Avella and F. Mancini (Springer, Berlin, 2015), pp. 205–235.
[5] F. J. García de Abajo, Rev. Mod. Phys. **82**, 209 (2010).
[6] F. Hofer, F. P. Schmidt, W. Grogger, and G. Kothleitner, IOP Conf. Ser.: Mater. Sci. Eng. **109**, 012007 (2016).
[7] R. H. Ritchie and A. Howie, Philos. Mag. A **58**, 753 (1988).
[8] R. F. Egerton, *Electron Energy-Loss Spectroscopy in the Electron Microscope* (Springer, Berlin, 2011).
[9] B. A. Lippmann and J. Schwinger, Phys. Rev. **79**, 469 (1950).
[10] E. Dagotto, Rev. Mod. Phys. **66**, 763 (1994).
[11] H. B. Schüttler and D. J. Scalapino, Phys. Rev. B **34**, 4744 (1986).
[12] A. W. Sandvik, Phys. Rev. B **57**, 10287 (1998).
[13] R. N. Silver, D. S. Sivia, and J. E. Gubernatis, Phys. Rev. B **41**, 2380 (1990).
[14] J. E. Gubernatis, M. Jarrell, R. N. Silver, and D. S. Sivia, Phys. Rev. B **44**, 6011 (1991).
[15] O. F. Syljuåsen, Phys. Rev. B **78**, 174429 (2008).
[16] S. Fuchs, T. Pruschke, and M. Jarrell, Phys. Rev. E **81**, 056701 (2010).
[17] A. W. Sandvik, Phys. Rev. E **94**, 063308 (2016).
[18] H. Shao, Y. Q. Qin, S. Capponi, S. Chesi, Z. Y. Meng, and A. W. Sandvik, Phys. Rev. X **7**, 041072 (2017).
[19] K. A. Hallberg, Phys. Rev. B **52**, R9827 (1995).
[20] T. D. Kühner and S. R. White, Phys. Rev. B **60**, 335 (1999).
[21] E. Jeckelmann, Phys. Rev. B **66**, 045114 (2002).
[22] A. J. Daley, C. Kollath, U. Schollwöck, and G. Vidal, J. Stat. Mech. (2004) P04005.
[23] S. R. White and A. E. Feiguin, Phys. Rev. Lett. **93**, 076401 (2004).
[24] A. E. Feiguin and S. R. White, Phys. Rev. B **72**, 020404(R) (2005).
[25] A. E. Feiguin, in *XV Training Course in the Physics of Strongly Correlated Systems*, AIP Conf. Proc. No. 1419 (AIP, Melville, NY, 2011), p. 5.
[26] A. E. Feiguin, in *Strongly Correlated Systems: Numerical Methods*, edited by A. Avella and F. Mancini (Springer, Berlin, 2013).
[27] S. Paeckel, T. Köhler, A. Swoboda, S. R. Manmana, U. Schollwöck, and C. Hubig, Ann. Phys. (NY) **411**, 167998 (2019).
[28] A. Holzner, A. Weichselbaum, I. P. McCulloch, U. Schollwöck, and J. von Delft, Phys. Rev. B **83**, 195115 (2011).
[29] F. A. Wolf, J. A. Justiniano, I. P. McCulloch, and U. Schollwöck, Phys. Rev. B **91**, 115144 (2015).
[30] H. D. Xie, R. Z. Huang, X. J. Han, X. Yan, H. H. Zhao, Z. Y. Xie, H. J. Liao, and T. Xiang, Phys. Rev. B **97**, 075111 (2018).
[31] L. Vanderstraeten, M. Mariën, F. Verstraete, and J. Haegeman, Phys. Rev. B **92**, 201111(R) (2015).
[32] L. Vanderstraeten, F. Verstraete, and J. Haegeman, Phys. Rev. B **92**, 125136 (2015).
[33] T. Li and F. Yang, Phys. Rev. B **81**, 214509 (2010).
[34] B. Dalla Piazza, M. Mourigal, N. B. Christensen, G. J. Nilsen, P. Tregenna-Piggott, T. G. Perring, M. Enderle, D. F. McMorrow, D. A. Ivanov, and H. M. Rønnow, Nat. Phys. **11**, 62 (2014).
[35] F. Ferrari, A. Parola, S. Sorella, and F. Becca, Phys. Rev. B **97**, 235103 (2018).
[36] D. Hendry and A. E. Feiguin, Phys. Rev. B **100**, 245123 (2019).
[37] K. Zawadzki and A. E. Feiguin, Phys. Rev. B **100**, 195124 (2019).
[38] J. K. Freericks, H. R. Krishnamurthy, and T. Pruschke, Phys. Rev. Lett. **102**, 136401 (2009).
[39] C. Shao, T. Tohyama, H.-G. Luo, and H. Lu, Phys. Rev. B **93**, 195144 (2016).
[40] K. Zawadzki, A. Nocera, and A. E. Feiguin, arXiv:2002.04142.
[41] J. des Cloizeaux and J. J. Pearson, Phys. Rev. **128**, 2131 (1962).
[42] G. Müller, H. Thomas, H. Beck, and J. C. Bonner, Phys. Rev. B **24**, 1429 (1981).
[43] A. Zheludev, M. Kenzelmann, S. Raymond, T. Masuda, K. Uchinokura, and S.-H. Lee, Phys. Rev. B **65**, 014402 (2001).
[44] M. B. Stone, D. H. Reich, C. Broholm, K. Lefmann, C. Rischel, C. P. Landee, and M. M. Turnbull, Phys. Rev. Lett. **91**, 037205 (2003).
[45] M. Kenzelmann, Y. Chen, C. Broholm, D. H. Reich, and Y. Qiu, Phys. Rev. Lett. **93**, 017204 (2004).
[46] M. Kohno, Phys. Rev. Lett. **102**, 037203 (2009).
[47] B. Lake, A. M. Tsvelik, S. Notbohm, D. Alan Tennant, T. G. Perring, M. Reehuis, C. Sekar, G. Krabbes, and B. Büchner, Nat. Phys. **6**, 50 (2010).
[48] P. Bouillot, C. Kollath, A. M. Läuchli, M. Zvonarev, B. Thielemann, C. Rüegg, E. Orignac, R. Citro, M. Klanjšek, C. Berthier, M. Horvatić, and T. Giamarchi, Phys. Rev. B **83**, 054407 (2011).
[49] D. Schmidiger, P. Bouillot, T. Guidi, R. Bewley, C. Kollath, T. Giamarchi, and A. Zheludev, Phys. Rev. Lett. **111**, 107202 (2013).
[50] D. Schmidiger, S. Mühlbauer, A. Zheludev, P. Bouillot, T. Giamarchi, C. Kollath, G. Ehlers, and A. M. Tsvelik, Phys. Rev. B **88**, 094411 (2013).
[51] F. Casola, T. Shiroka, A. Feiguin, S. Wang, M. S. Grbić, M. Horvatić, S. Krämer, S. Mukhopadhyay, K. Conder, C. Berthier, H.-R. Ott, H. M. Rønnow, C. Rüegg, and J. Mesot, Phys. Rev. Lett. **110**, 187201 (2013).
[52] M. Mourigal, M. Enderle, A. Klöpperpieper, J.-S. Caux, A. Stunault, and H. M. Rønnow, Nat. Phys. **9**, 435 (2013).
[53] D. Blosser, N. Kestin, K. Y. Povarov, R. Bewley, E. Coira, T. Giamarchi, and A. Zheludev, Phys. Rev. B **96**, 134406 (2017).
[54] S. Ward, M. Mena, P. Bouillot, C. Kollath, T. Giamarchi, K. P. Schmidt, B. Normand, K. W. Krämer, D. Biner, R. Bewley, T. Guidi, M. Boehm, D. F. McMorrow, and C. Rüegg, Phys. Rev. Lett. **118**, 177202 (2017).
[55] W. J. Gannon, I. A. Zaliznyak, L. S. Wu, A. E. Feiguin, A. M. Tsvelik, F. Demmel, Y. Qiu, J. R. D. Copley, M. S. Kim, and M. C. Aronson, Nat. Commun. **10**, 1123 (2019).
[56] W. Yang, J. Wu, S. Xu, Z. Wang, and C. Wu, Phys. Rev. B **100**, 184406 (2019).
[57] A. Keselman, L. Balents, and O. A. Starykh, Phys. Rev. Lett. **125**, 187201 (2020).
[58] F. Essler, H. Frahm, F. Göhmann, A. Klümper, and V. E. Korepin, *The One-Dimensional Hubbard Model* (Cambridge University Press, Cambridge, 2010).
[59] T. Oka and H. Aoki, Phys. Rev. B **78**, 241104(R) (2008).

[60] M. Kohno, Phys. Rev. Lett. **105**, 106402 (2010).
[61] M. Kohno, Phys. Rev. Lett. **108**, 076401 (2012).
[62] A. Nocera, F. H. L. Essler, and A. E. Feiguin, Phys. Rev. B **97**, 045146 (2018).
[63] C. Yang and A. E. Feiguin, Phys. Rev. B **93**, 081107(R) (2016).
[64] T. E. Kidd, T. Valla, P. D. Johnson, K. W. Kim, G. D. Gu, and C. C. Homes, Phys. Rev. B **77**, 054503 (2008).
[65] H. Matsueda, N. Bulut, T. Tohyama, and S. Maekawa, Phys. Rev. B **72**, 075136 (2005).
[66] M. M. Zemljic, P. Prelovsek, and T. Tohyama, Phys. Rev. Lett. **100**, 036402 (2008).
[67] M. Eckstein and P. Werner, Phys. Rev. Lett. **110**, 126401 (2013).
[68] M. Eckstein and P. Werner, Phys. Rev. Lett. **113**, 076405 (2014).
[69] K. Balzer, F. A. Wolf, I. P. McCulloch, P. Werner, and M. Eckstein, Phys. Rev. X **5**, 031039 (2015).
[70] D. Golež, M. Eckstein, and P. Werner, Phys. Rev. B **92**, 195123 (2015).
[71] N. Bittner, D. Golež, H. U. R. Strand, M. Eckstein, and P. Werner, Phys. Rev. B **97**, 235125 (2018).
[72] M. Raczkowski, F. F. Assaad, and L. Pollet, Phys. Rev. B **91**, 045137 (2015).